Effective potential energies and transport cross sections for interactions of hydrogen and nitrogen

James R. Stallcop and Harry Partridge
NASA Ames Research Center, MS 230-3, Moffett Field, California 94035-1000

Eugene Levin
Eloret Corporation, MS 230-3, Moffett Field, California 94035-1000
(Received 1 May 2000; published 9 November 2000)

The interaction energies for N_2-He and N_2-H_2 are calculated by accurate *ab initio* methods. The virial coefficient and differential scattering cross section for N_2-H_2 are calculated; the theoretical results are compared with experimental data. The transport collision integrals for N_2-H_2 and N_2-N_2 interactions are calculated and tabulated; the results yield transport coefficients that compare well with measured data. Transport coefficients are found to be determined accurately from the interaction energies for a specific configuration of the molecule formed from the interaction partners. Comparisons with results of measurement and accurate calculations demonstrate that the transport properties of complex molecular interactions can be determined rapidly and fairly accurately from the interaction energies of simpler systems using combination rules for the short-range parameters of effective interaction energies and the coefficients for the long-range forces. The coefficients for a two-parameter temperature expansion of diffusion and viscosity are tabulated for a realistic universal potential-energy that is based primarily on the results of very accurate calculations of the He-He interaction energy.

PACS number(s): 34.20.Mq

I. INTRODUCTION

The transport properties of the interaction of hydrogen and nitrogen are required for studies of certain hydrogen-burning propulsion systems and the corresponding environment of their space vehicles. The H-N and N-N interaction energies for the states of the molecule that correspond to dissociation into ground-state atoms have been calculated [1–3] and the results have been applied to determine the transport collision integrals for these systems. Similarly, the potential-energy surfaces for the interactions H_2-H, N_2-H, and N_2-N_2 have been determined [4–7] and used to obtain [6,8] the transport integrals for the atom-molecule collisions. In addition, we have tabulated [9] the collision integrals for H-H and H_2-H_2 interactions that were calculated from accurate interaction energies. We have also calculated the interaction energies and transport data for H_2-N and N_2-N collisions [10]. In the present work, we calculate interaction energies of the unlike systems N_2-He and N_2-H_2 and tabulate the collision integrals for N_2-H_2 and N_2-N_2. The present work completes the transport database required for interactions between all the neutral atoms and diatomic homonuclear molecules of hydrogen and nitrogen.

The calculation of potential energies required for conventional determinations of transport properties can be a very laborious task. Moreover, these calculations become impractical for systems involving the interactions of large molecules, such as those required for studying or modeling the deposition and etching processes for the manufacturing [11] of microelectronic devices. In this study, we apply molecular symmetry to identify effective potential energies that yield accurate approximations to those transport properties such as diffusion and viscosity that are dominated by elastic scattering processes. Furthermore, we present a realistic two-parameter universal transport formulation that is based on the results of accurate *ab initio* calculation of interaction energies and is compatible with a transport database consisting of potential parameters. Finally, we illustrate that effective potential energies for complex systems can be readily predicted from the interaction energies for simpler systems, such as those involving He, using combination rules for the repulsive energy and the long-range interaction coefficients.

The determination of the interaction energies is described in Sec. II. The application of the molecular interaction energies to the determination of virial coefficients, scattering cross sections, and transport data is contained in Sec. III. Approximations to reduce the computational effort required to determine transport data are examined in Sec. IV. Finally, conclusions can be found in Sec. V

II. MOLECULAR INTERACTION ENERGIES

A. Atom-molecule interactions

The geometry for atom-homonuclear molecule orientations is specified [12] in terms of the separation distance r, from the center of the atom to the center of mass of the homonuclear diatomic molecule, and the angle θ between a line joining the center of the atom with the center of mass of the molecule and the molecular symmetry axis passing through the nuclear centers.

The potential-energy surface describing atom-homonuclear molecule interactions for a fixed internuclear separation distance can be accurately represented using the expansion

$$V(r,\theta)=\sum_{n=0} v_{2n}(r)P_{2n}(\cos\theta), \tag{1}$$

where $P_{2n}(\cos\theta)$ is a Legendre polynomial.

For small anisotropy, the spherically averaged potential $v_0(r)$ can be determined from the orientation [6,8] specified by the angle

$$\theta_0 = \cos^{-1}(1/\sqrt{3}) \approx 54.735\,610°, \tag{2}$$

for which $P_2(\cos\theta_0)$ vanishes. Similarly, quantities such as transport cross sections that vary slowly with θ can be calculated with reasonable accuracy [6,8,10] from the interaction energies for the orientation specified by θ_0. Hence, $V(r,\theta_0)$ can be considered to be an effective spherical potential for the determination of transport cross sections.

We calculate the He-N_2 rigid-rotor potential-energy for the θ_0 orientation accurately using a high-level quantum chemistry method in order to investigate the validity of the approximations of Sec. IV. Specifically, a coupled-cluster singles and doubles approach [13] that includes a perturbational correction [14] for triples [CCSD(T)] is combined with large basis sets; the atom-centered wave functions are obtained from the augmented correlation-consistent polarized-valence quadruple zeta (aug-cc-pVQZ) of Dunning and co-workers [15–17]. Vladimiroff [18] and Burton *et al.* [19] have shown that significantly lower energies can be readily achieved by adding bond functions to the basis set. The rate of convergence of calculations that take the basis-set superposition error (BSSE) into account has been examined for both strong [20,21] and weak [22,23] molecular binding. Reliable values of the potential-energy can be obtained [22,23] by using computational methods that correct for BSSE. Midpoint-centered bond functions [22] are included in the present calculation and the counterpoise method [24] is used to remove BSSE.

Our calculated values for $V(r,\theta_0)$ are shown in Fig. 1 for large values of r. Note that our values lie only slightly lower than the corresponding values that are interpolated from the results of the fourth-order Møller-Plesset perturbation (MP4) calculations of Hu and Thakkar [25] using Eq. (1). Certain effective potential energies that are deduced from experimental data are also compared with the theoretical results in Fig. 1. We show that a potential energy that reproduces [26,27] the measured viscosity data has a potential well that is considerably deeper than that of the *ab initio* calculations; this comparison illustrates that viscosity data for a narrow range [26] of high temperatures T alone is not sufficient to determine a meaningful effective potential energy at large r. Contrarily, the effective potential-energy from the correlation of Bzowski *et al.* [28] that reproduces measured data for both the second virial coefficient $B(T)$ and the transport data agrees fairly well with the theoretical results.

The *ab initio* results are extended to larger r using a long-range expansion of the interaction energy. The orientation-averaged leading dispersion energy $\overline{C_6}$ obtained from measured photoabsorption cross sections and other data by Meath and Kumar [29] is $10.23ea_0^2$. The higher-order dispersion coefficients can be obtained from the results of the perturbation calculation of Hettema *et al.* [30]. The small contribution from the induction terms can be determined from the formulation of Ref. [30] using the polarizabilities of the atom and multipole moments of the molecule. The polarizabilities of He have been calculated [31] accurately; the measured values of the quadrupole moment Q_2 and the hexadecapole moment Q_4 of N_2 are $-1.04ea_0^2$ [32] and $-8.5ea_0^4$ [33], respectively. The results of the present calculation agree well with the corresponding results of the long-range expansion. For example, at $r=10$, the values of *ab initio* energy $V^c(r,\theta_0)$ and the long-range expansion $V_{\rm LR}(r,\theta_0)$ are $-12.8\mu E_h$ and $-13.0\mu E_h$, respectively. We estimate that the short-range exchange repulsion [34] contributes about $0.1\mu E_h$; hence, the actual difference between the *ab initio* and long-range energies is only about $0.1\mu E_h$.

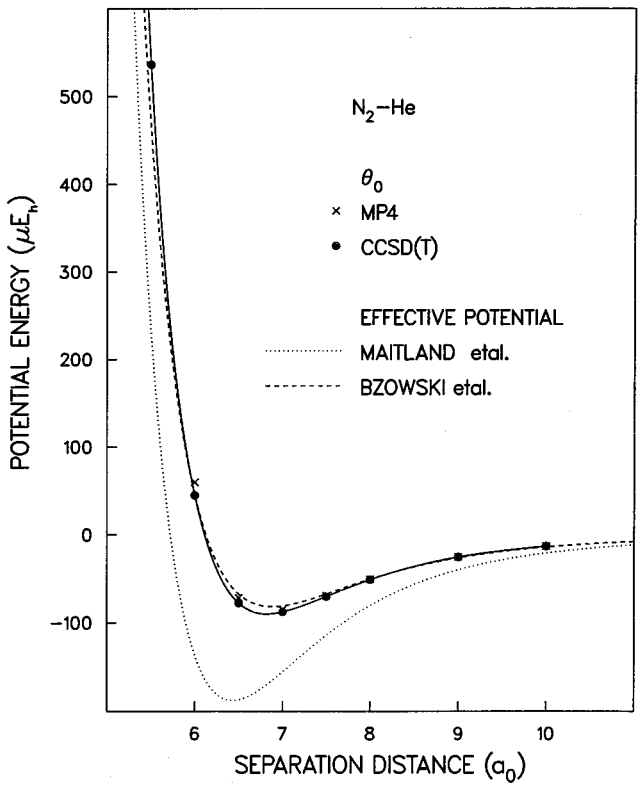

FIG. 1. N_2-He potential-energy curves at large r. The solid circles represent the calculated results at θ_0 from the present work and the crosses represent the results of Ref. [25] as described in the text. The solid curve was obtained from a spline fit to the present calculation. The dotted and dashed curves represent the potential curves of Refs. [27] and [28], respectively.

The interaction potential for small r is required for the calculation of transport properties at high collision energies E. Since the N_2-He interaction energy has a van der Waals minimum at large r, the potential-energy function developed by Tang and Toennies [35] for atom-atom interactions can be adapted for the analysis [4] of the repulsive energy for interactions involving molecules. The general form of the modified Tang-Toennies potential-energy function $V_{\rm MTT}(r,\boldsymbol{\omega})$ for collisions involving molecules has been applied successfully in previous work [4,8,7] and is outlined in Appendix A. The *ab initio* interaction energies $V^c(r,\boldsymbol{\omega})$ are analyzed using the short-range repulsive energy

$$V^c_{\rm SR}(r,\boldsymbol{\omega}) = V^c(r,\boldsymbol{\omega}) - V_{\rm DLR}(r,\boldsymbol{\omega}), \tag{3}$$

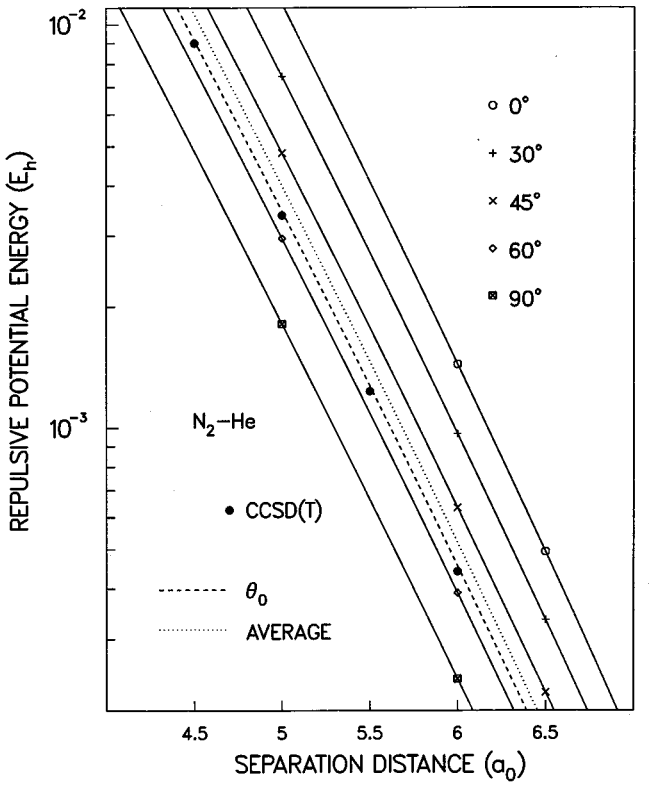

FIG. 2. N_2-He repulsive potential-energy curves at small r. The full circles are obtained from the results of the present calculation at θ_0. The data points for the angles 0°,45°, and 90° were obtained from the calculated results of Ref. [25]; the data points for 30°,60°, and the dotted and dashed curves [for $v_0(r)$ and $V(r,\theta_0$, respectively] were determined from the fit of Eq. (1) to the calculated results of Ref. [25]. All curves were obtained from spline fits to the data.

where $V_{\mathrm{DLR}}(r,\boldsymbol{\omega})$ is obtained from the long-range coefficients described above and the short-range repulsive parameter ρ, as described in Appendix A, using Eqs. (A1c) and (A1d). For atom-homonuclear interactions such as those considered here, $\boldsymbol{\omega}$ is specified simply by the angle θ. The quantity ρ is calculated using the iterative procedure outlined in Appendix A.

The values of $\ln V^c_{\mathrm{SR}}(r,\theta)$ are displayed in Fig. 2. The linear behavior of the curves shown in Fig. 2 indicates that $V^c_{\mathrm{SR}}(r,\boldsymbol{\omega})$ for fixed θ can be described well by an exponential function for a broad range of r and, consequently, that the potential-energy data could be represented well by V_{MTT} as in Refs. [4], [6], and [10]. Note that the results of the present calculation lie slightly lower than the corresponding results of Ref. [30] in Fig. 1. The uniform variation of the curves for the selected values of θ indicates [6] that $V^c_{\mathrm{SR}}(r,\theta)$ primarily exhibits the simple behavior described by a polynomial expansion of the form (1) with only two terms. This observation is confirmed by the small difference between $V^c(r,\theta_0)$ and $v_0(r)$, which indicates that there is only a small contribution from the higher-order $P_n(\cos\theta)$ for $n>2$.

The small differences between the present data and the corresponding results obtained from Ref. [25] shown in Figs. 1 and 2 indicate that results of the MP4 approximation yield a global potential-energy that is satisfactory for the comparisons of Sec. IV.

B. Molecule-molecule interactions

For this work, the potential-energy for the interaction of homonuclear diatomic molecules is specified [7] by the following coordinates. The length r is the separation distance between the center of mass of the H_2 molecule and the center of mass of the N_2 molecule. The angles θ_a and θ_b specify the orientation of the symmetry axis of the H_2 molecule and the N_2 molecule, respectively, with respect to the z axis passing through the center of mass of each molecule. The angle ϕ is the difference between the azimuthal angles, i.e.,

$$\phi=\phi_a-\phi_b\,. \tag{4}$$

The potential-energy can be expanded in polynomials [7],

$$V(r,\theta_a,\theta_b,\phi)=\sum\, c_{L_aL_bM}d_{L_aL_bM}(\theta_a,\theta_b,\phi), \tag{5}$$

where only zero or even values of L_a and L_b are allowed when the functions $d_{L_aL_bM}$ are represented [7] by spherical harmonics, i.e.,

$$d_{L_aL_bM}(\theta_a,\theta_b,\phi)=P_{L_aM}(\cos\theta_a)P_{L_bM}(\cos\theta_b)\cos(M\phi), \tag{6}$$

where $P_{L,M}$ is an associated Legendre polynomial.

The determination of the complete potential-energy surface requires a large computational effort. For interactions of like molecules, Koida and Kihara [36] have shown that nine orientations are sufficient to approximate the spherical average of quantities that can be represented by expansions (5) for $L\leqslant 4$ using the relation found on p. 45 of Ref. [36]. In Appendix B, we show that the extension of their approach to include interactions between unlike molecules requires an additional three orientations. The angles that specify all of the required orientations to determine spherically averaged quantities using the equivalent Koida-Kihara approximation for unlike molecules (KKU) expressed by Eq. (B11) are described in Table I.

The N_2-H_2 potential energies are computed for the orientations of Table I using *ab initio* methods, which are described in Refs. [37] and [7]. These results are extended to large r for the applications described in Sec. III using long-range expansions of the interaction energy. The major contribution to the electrostatic energy can be obtained using the multipole formulation of Ref. [38] and the multipole moments of the molecules. The moments for H_2 have been calculated accurately; the values of Q_2 and Q_4 are $0.483ea_0^2$ [39] and $0.321ea_0^4$ [40], respectively.

The long-range dispersion coefficients can be expressed in the form

$$C^{\nu}(\boldsymbol{\omega})=C^{\nu}_{000}\left[1+\sum\,\gamma^{\nu}_{L_aL_bM}d_{L_aL_bM}(\boldsymbol{\omega})\right], \tag{7}$$

TABLE I. KKU orientations for homonuclear molecules. (The KK orientations required for the interaction of like molecules are listed above. The angles of the orientations xz, dz, and dx required for interactions of unlike molecules are obtained by simply interchanging the values of θ_a and θ_b for zx, zd, and xd, respectively.)

Notation	θ_a	θ_b	ϕ
zz	0	0	
zx	0	$\pi/2$	
xx	$\pi/2$	$\pi/2$	0
xy	$\pi/2$	$\pi/2$	$\pi/2$
zd	0	θ_0	
xd	$\pi/2$	θ_0	$\pi/4$
dd	θ_0	θ_0	0
dd'	θ_0	θ_0	$\pi/2$
dd''	θ_0	θ_0	π

where the quantities C^{ν}_{000} are the long-range coefficients of the spherically averaged potential-energy $\overline{V}(r)$. The values of $\gamma^{\nu}_{L_aL_bM}$ for the body-fixed frame of the present work are obtained from the calculated results of Refs. [41] and [42] for a space-fixed frame using the transformation of Ref. [41]. The value [29] selected for the leading coefficient C^6_{000} is $29.46a_0^6E_h$. The values of the higher-order C^{ν}_{000} are obtained from Refs. [41] and [42].

The formulation of Appendix A is applied to determine $V^c_{\rm SR}(r,\boldsymbol{\omega})$ using Eq. (3) from the *ab initio* data for $V^c(r,\boldsymbol{\omega})$ and the long-range interaction energies as described above. For the interaction of homonuclear molecules, $\boldsymbol{\omega}$ is specified by the angles θ_a, θ_b, and ϕ. The results for $\ln V_{\rm SR}(r,\boldsymbol{\omega})$ are shown in Fig. 3 for the KKU orientations. Again the linear behavior of the curves of Fig. 3 indicates an exponential behavior for $V^c_{\rm SR}(r,\boldsymbol{\omega})$ for fixed $\boldsymbol{\omega}$ as found in Ref. [7]. The result obtained from the $\overline{V}(r)$ that is calculated from the $V^c(r,\boldsymbol{\omega})$ using the approximation (B11) and the C^{ν}_{000} described above is also shown for comparison. Note that the result obtained from $\overline{V}(r)$ lies slightly above the corresponding result that is obtained from the potential-energy $V_{dd'}(r)$ for the dd' configuration. Analogous to the atom-molecule comparison discussed above, one concludes from the results of Appendix B that the contributions from the higher-order polynomials $P_{L,M}$ for $L>2$ produce a larger repulsion than that found for the approximate potential-energy obtained from Eq. (B10) for a truncation with $L\leqslant 2$.

The potential-energy surface for N_2-N_2 interactions has been constructed by adjusting [7] the results of *ab initio* calculations to yield agreement with measured values of $B(T)$. The modified energies were obtained from a small rotation [7] of $V^c_{\rm SR}(r,\boldsymbol{\omega})$ with the angular variation constrained by the results of calibration calculations with large basis sets. More accurate recent *ab initio* calculations [43] that use bond functions in a manner similar to that described above for the present He-N_2 calculations yield interaction energies that are only slightly lower at small r, but significantly lower in the region of the van der Waals minimum at large r than the corresponding energies of the *ab initio* calculations of Ref. [7]. The energies of the improved calculations [43] agree well with the modified potential energies of Ref. [7]. The agreement is illustrated by Fig. 4, where the computed values of $V(r,\boldsymbol{\omega})$ of Ref. [43] are compared with the corresponding results for the potential-energy surface obtained by the VS method [7] (where the variation in ρ is determined using the results of calculations with larger basis sets) for the various orientations of Fig. 2 of Ref. [7]. The VS potential-energy surface is applied in Secs. III and IV below.

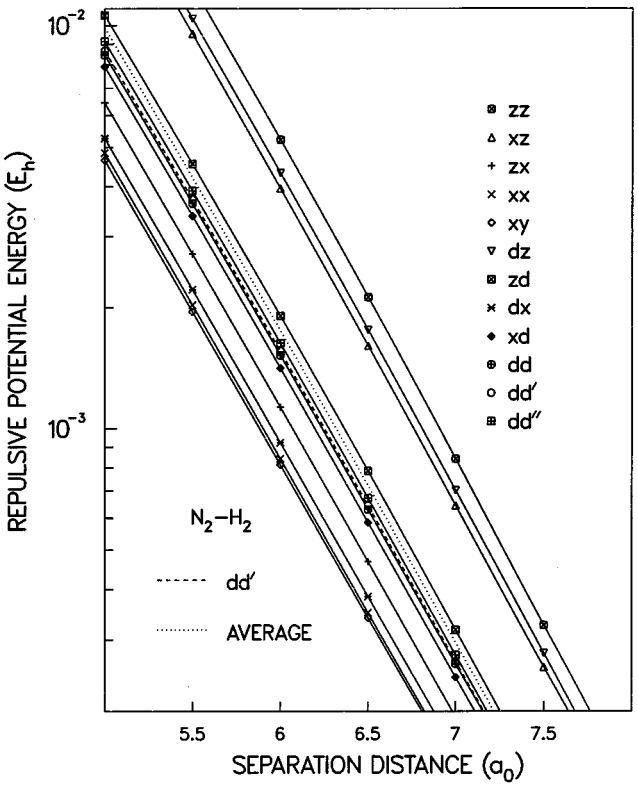

FIG. 3. Repulsive potential-energy curves for N_2-H_2 interactions for the orientations defined in Table I. The data points are determined from the *ab initio* results; all curves are obtained from spline fits to the data. The dd' orientation is represented by a dashed curve; the results for all other orientations are displayed by solid curves. The dotted curve is determined from $\overline{V}(r)$.

The scattering calculations of the present work depend primarily on the repulsive region of the potential energies. We consider effective spherical potential energies for molecule-molecule interactions that are analogous to those discussed above for atom-molecule interactions. The values of $\overline{V}(r)$, a choice for the calculation of high-T transport data [28,44], and $V_{dd'}(r)$, selected by Eq. (B10) to obtain averages of quantities with a small anisotropy, that are determined from the results of *ab initio* calculations for the interactions of hydrogen and nitrogen molecules are shown in Fig. 5. We note the the curves for $\overline{V}(r)$ lie above the corresponding curves for $V_{dd'}(r)$ for all the interactions. The two curves are nearly the same for H_2-H_2, where the interaction potential energy has a small anisotropy, but are well separated for the other two interactions, which have large anisotropies.

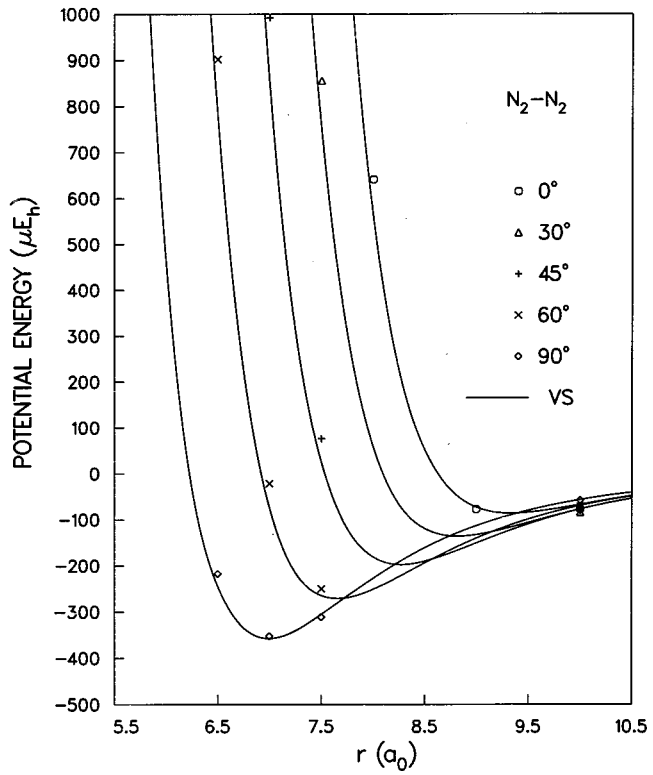

FIG. 4. Comparison of N_2-N_2 potential energies for r in the region of the van der Waals minimum at $dd''(\theta)$ orientations [7] for the various values of the angle θ listed in the figure. The solid curves are determined from the VS results [7]; the data points are the results from the *ab initio* calculation of Ref. [43].

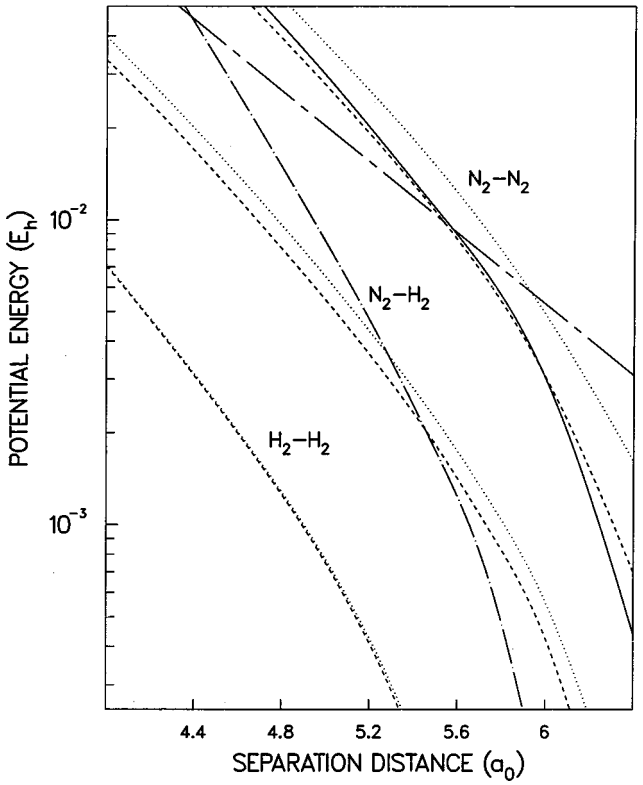

FIG. 5. Effective potential energies for the interactions of the molecules of hydrogen and nitrogen at small r. The dashed and dotted curves represent $V_{dd'}(r)$ and $\overline{V}(r)$, respectively. The solid, long- and short-dashed, and the dash-dotted curve were determined from the interaction energies of Refs. [46], [44], and [45], respectively, which were deduced, primarily, from measured data as described in the text.

The results are also compared in Fig. 5 with interaction energies that were deduced from experimental results. We show the spherical interaction energy curves [45] that reproduce the measured values of the N_2-H_2 differential scattering cross sections and also the N_2-N_2 result [28,44] obtained from the values of $\overline{V}(r)$ that were deduced from measured cross-section data using combination rules. Similarly, we show an effective N_2-N_2 interaction energy that reproduces [46] the measured data for $B(T)$, viscosity $\eta(T)$, and differential scattering cross sections. Note that the results of Ref. [46] agree fairly well with the corresponding curve for $V_{dd'}(r)$.

III. APPLICATIONS OF THE MOLECULAR INTERACTION ENERGIES

A. Second virial coefficient

At low T, the quantity $B(T)$ is sensitive to the anisotropy of V at large r. We use semiclassical approximations for $B(T)$ that are obtained from an expansion in $\hbar$; the KK or KKU approximations described above may be applied for each of the terms of this expansion. The first-order corrections to the classical value $B_0(T)$ are obtained using the formulation of Pack [47].

The global potential-energy surface for N_2-N_2 of Ref. [7] is applied to investigate the accuracy of the KK approximation for $B(T)$ when the anisotropy of the molecular interaction is large. We find that the errors in $B_0(T)$ and $B(T)$ introduced by the KK approximation are only about 0.04% and 0.14%, respectively, at 75 K (the lowest value of T of the measurements applied to construct [7] the potential surface) and decrease with increasing T. The largest contribution to the error comes from the first-order correction $B_{1a}(T)$, which is determined from the angular derivatives of V. We conclude that the KK approximations would be adequate for an analysis [7] of the measured data for $B(T)$ since the experimental uncertainties are considerably larger than the KK errors.

The N_2-H_2 potential energies calculated without BSSE corrections are applied to determine $B(T)$ using the KKU orientations of Table I and the approximation (B11). The second-order radial contribution $B_{2r}(T)$ is included using the result obtained by adapting the central-field formulation of Ref. [38]. The results are compared with measured data in Fig. 6. Adding the BSSE correction would raise the curve for the calculated result slightly; on the other hand, the contribution from the neglected term for $B_{2a}(T)$ would lower the curve. The additional effort required to obtain higher-order terms of the semiclassical expansion would not necessarily yield a more meaningful comparison with the experimental data, since the measured results most likely

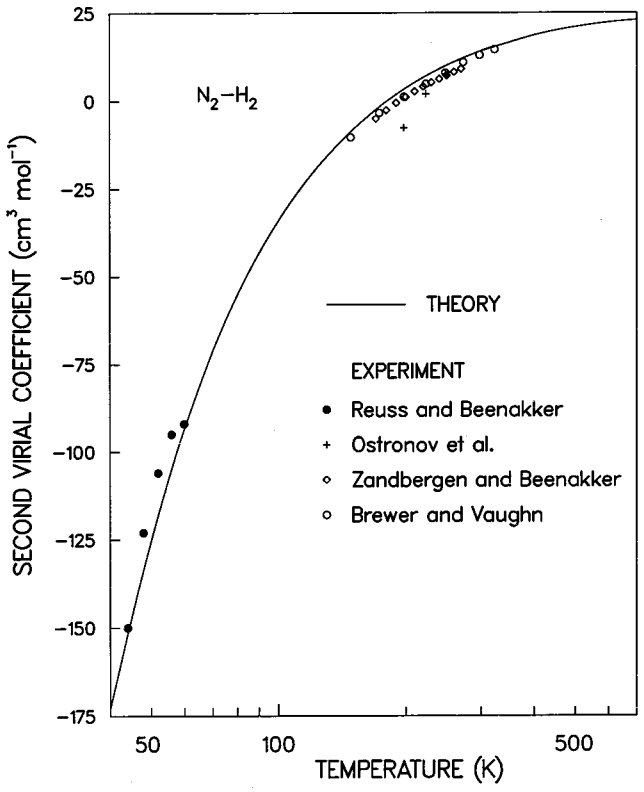

FIG. 6. The second virial coefficient for N_2-H_2 interactions. The points represent the measurements of Refs. [48–51]. The solid curve was obtained from the present calculations as described in the text.

contain contributions from molecular dimers [52], which are difficult to determine, but can be significant at the lower T of Fig. 6.

B. Scattering calculations

The major contribution to the scattering at small scattering angles comes from collisions with large impact parameters; since the distance of closest approach is large and the molecular collision partners are rotating during the collision, $\overline{V}(r)$ is expected to provide a good approximation to the small-angle differential scattering cross sections. In Appendix C, we show that the scattering approximation of Parker and Pack [53], which was derived using both centrifugal and energy sudden approximations, yields cross sections that are nearly the same as those determined from $\overline{V}(r)$ if the anisotropy of the long-range coefficients for the interaction of the collision partners is small (e.g., the values of γ are small). At smaller impact parameters where a semiclassical approximation to the scattering is valid, the major contribution to scattering comes from the region of the closest distance of approach [27]. Hence, the sudden approximation is expected to yield reasonable approximations to differential scattering cross sections for nearly all scattering angles and, consequently, to the total scattering cross sections, such as those required for the determination of transport properties for the interactions considered in this paper. In addition, we point out that the values of C^{ν} for the dd' orientation are nearly the same as those for $\overline{V}(r)$ if the γ for large L are small; hence, the small-angle scattering cross sections for the dd' orientation are expected to provide a reasonable approximation to the corresponding observed results.

In this work, scattering cross sections that represent the contribution from all orientations of the collision partners are determined from the interaction energies of Sec. II that contain corrections for BSSE using sudden approximations [53]. A quantum-mechanical description is used to determine the scattering in the central field $V(r,\boldsymbol{\omega})$ for the orientation specified by $\boldsymbol{\omega}$. The scattering phase shift $\eta_l(E)$ for each angular momentum quantum number l is calculated at lower E from a numerical integration of the Schrödinger equation, using the method presented by Levin *et al.* [54]. A semiclassical method [55] is used to determine $\eta_l(E)$ at E above a threshold energy E_t where the difference in the cross sections between the two methods does not exceed 0.3%. (Hence, there is a small uncertainty in the cross sections of the present calculation for a small range of E above E_t.)

1. N_2-H_2 *differential scattering cross sections*

The N_2-H_2 differential scattering cross section is calculated for each of the KKU orientations of Table I; the approximation (B11) is then used to obtain the cross sections that would be observed in the laboratory. The computed results for the peak velocity of the experiment of Miller *et al.* [45] are compared with measured cross sections in Fig. 7. The calculated results represent high-resolution cross sections in that we have not averaged the results over the spread [45] of the beam velocities. The measured cross sections [45] of Fig. 7 are obtained using the transformation from the laboratory system to the center of mass system described in Ref. [56]. We also show the results calculated from $\overline{V}(r)$ and $V_{dd'}(r)$. Note that the cross section for $\overline{V}(r)$ agrees well with the corresponding result from sudden approximations at small scattering angles; this agreement is explained by the analysis of Appendix C. The locations of the peaks and valleys in the theoretical cross section agree well with the measured results; an averaged cross section that takes the energy and angular spread of the beams as well as the angular resolution of the measuring device into account would have an appearance similar to the less pronounced structure exhibited by measured results.

2. *Transport collision integrals and properties*

We have shown that the sudden approximations [53] yield H-H_2 collision integrals that are accurate [8], i.e., our calculated values of the diffusion and viscosity coefficients agree with the corresponding results from close-coupling calculations to within 1%. The theoretical diffusion agrees well [6,8] with measurements at room temperature. Furthermore, we have shown that our calculated viscosity for H_2-H_2 collisions agrees well [8,9] with the corresponding measured results in the low-T region where the uncertainty in the experimental data is relatively small.

The transport cross sections $Q_n(E,\boldsymbol{\omega})$ for each orientation are determined from the η_l by the sum

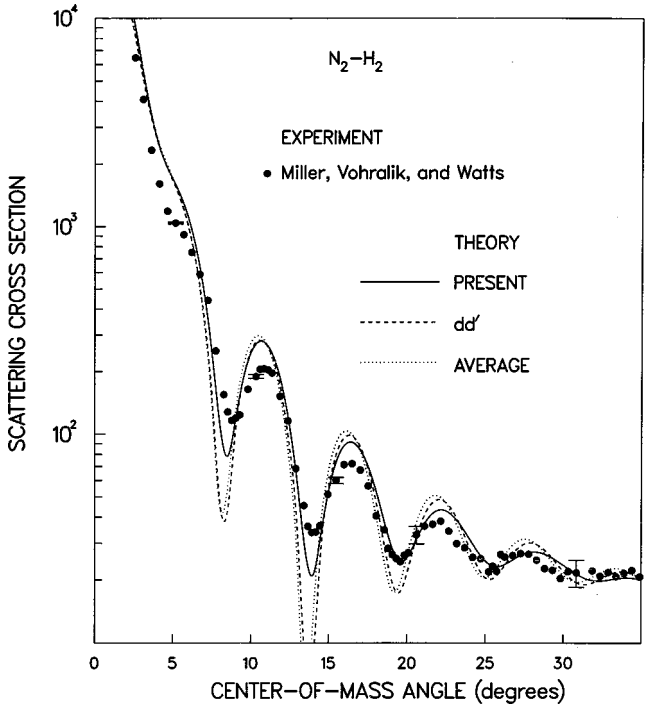

FIG. 7. Differential scattering cross section for N_2-H_2 interactions as a function of the scattering angle in the center of mass system. The points represent the experimental values of Ref. [45]; the stated uncertainties for the measurements are indicated by the error bars. Only relative values of the cross sections have been measured; the scale factor for the experimental cross sections is chosen to allow agreement of the calculated and measured values at large scattering angles. The dashed and dotted curves are calculated from $V_{dd'}(r)$ and $\overline{V}(r)$, respectively.

$$Q_n = \frac{4\pi}{k^2} \sum_{l=0}^{\infty} \sum_{\nu>0}^{n} a_{n\nu}^{l} \sin^2(\eta_{l+\nu} - \eta_l), \tag{8}$$

where k is the wave number, and the allowed values of ν are even or odd according to the parity of n. The coefficients $a_{n\nu}^{l}$ can be determined from recursion relations [2].

The cross sections $\overline{Q}_n(E)$ that would be observed in the laboratory are obtained from the appropriate integral [53] of $Q_n(E,\boldsymbol{\omega})$ over all orientations. The collision integrals are determined from an average [27] over a Maxwell-Boltzmann velocity distribution, i.e.,

$$\Omega_{n,s}(T) = \frac{F(n,s)}{2(\kappa T)^{s+2}} \int_0^{\infty} e^{-E/\kappa T} E^{s+1} \overline{Q}_n(E) dE, \tag{9}$$

where κ is the Boltzmann constant and $F(n,s)$ is a hard-sphere factor [2].

The values of $\overline{Q}_n(E)$ for N_2-H_2 are determined from the Q_n for the KKU orientations of Table I using the approximation (B11). Since we find that the values of $\overline{Q}_n(E)$ for N_2-N_2 obtained from the VS potential energies using the KK approximation are essentially the same as the results obtained by numerical integration over all orientations, we expect that the KKU orientations are sufficient to determine the N_2-H_2 transport cross sections with an accuracy that is smaller than the uncertainty in the *ab initio* energies.

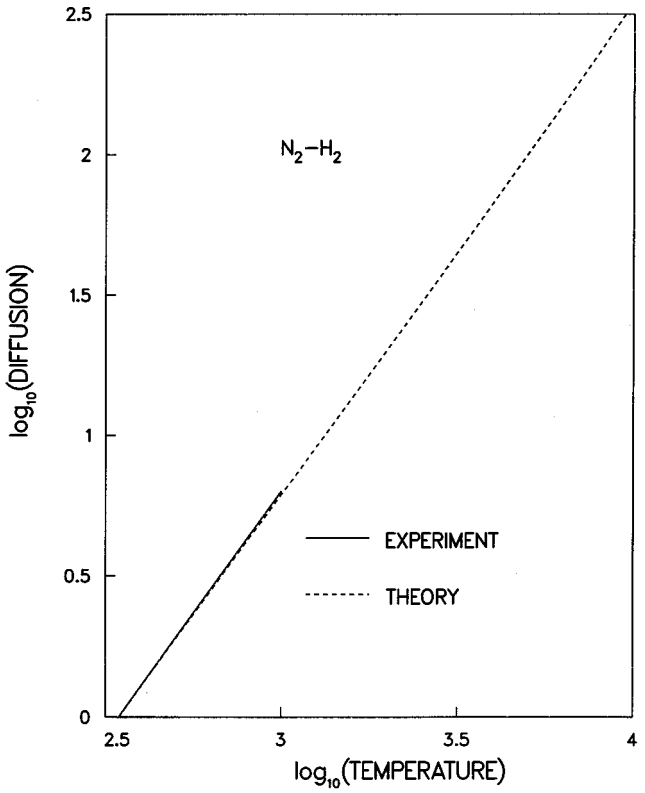

FIG. 8. The diffusion in units of cm^2/s as a function of temperature in K at a pressure of 1 atm for N_2-H_2 interactions. The solid line is determined from the second-order correlation of Ref. [60] for a 50/50 concentration of hydrogen and nitrogen. The dashed line is obtained from the present calculations as described in the text.

The values of $\Omega(T)$ for H_2-N_2, and N_2-N_2 are listed in Tables II and III, respectively; the tabulated quantities are required to determine transport properties for a mixture to second order [27]. The values of $\Omega(T)$ in Table III at low T have been obtained from a small adjustment of the corresponding calculated values to yield transport properties that agree with accurate measurements [57–59] of diffusion and viscosity. The values of the diffusion coefficient for N_2-H_2 that are calculated [38] from the Ω listed in Table II are shown in Fig. 8 and compared with the measured data, which are available at lower T. The calculated diffusion includes a small second-order mixture contribution [27] for the composition [60] selected for correlation of measured data. The calculated viscosity coefficient for N_2-N_2 is compared with the results of simple approaches in the following section.

IV. TRANSPORT APPROXIMATIONS

A. Effective potential energies

The identification of the effective potential-energy $V_e(r)$ that yields transport cross sections leads to substantial reduction in the computational effort required to determine transport data. For He-N_2 interactions, we find that $V(r,\theta_0)$ provides values of $V_e(r)$ that yield fairly accurate atom-

TABLE II. N_2-H_2 collision integrals (Å^2).

T (K)	$\Omega_{1,1}$	$\Omega_{1,2}$	$\Omega_{1,3}$	$\Omega_{1,4}$	$\Omega_{1,5}$	$\Omega_{2,2}$	$\Omega_{2,3}$	$\Omega_{2,4}$	$\Omega_{3,3}$
100	12.13	10.78	10.09	9.64	9.31	13.35	12.29	11.66	11.55
150	10.74	9.79	9.25	8.86	8.56	11.92	11.17	10.69	10.48
200	10.00	9.20	8.72	8.37	8.11	11.14	10.54	10.13	9.86
300	9.12	8.48	8.06	7.72	7.47	10.28	9.79	9.42	9.12
400	8.59	7.99	7.60	7.32	7.09	9.73	9.29	9.00	8.63
600	7.91	7.38	7.02	6.70	6.43	9.07	8.67	8.34	8.11
800	7.47	6.94	6.51	6.29	6.08	8.60	8.13	7.91	7.52
1000	7.12	6.62	6.26	5.98	5.74	8.26	7.88	7.58	7.25
1200	6.84	6.36	6.00	5.72	5.48	7.98	7.61	7.30	6.99
1500	6.51	6.04	5.68	5.40	5.16	7.64	7.26	6.96	6.66
2000	6.11	5.63	5.28	5.00	4.78	7.21	6.83	6.52	6.23
3000	5.53	5.07	4.73	4.46	4.23	6.60	6.23	5.92	5.66
4000	5.13	4.67	4.34	4.09	3.89	6.16	5.80	5.53	5.25
6000	4.59	4.15	3.85	3.57	3.34	5.59	5.25	4.93	4.73
8000	4.21	3.78	3.45	3.20	3.01	5.16	4.80	4.51	4.30
10000	3.92	3.49	3.18	2.93	2.71	4.84	4.48	4.19	4.00

homonuclear diatomic molecule transport cross sections, as in other work [6,8,10]. This is illustrated using the N_2-He diffusion cross section that is calculated in the sudden approximation; the results for the diffusion coefficient are compared with the measured data in Fig. 9.

The molecular viscosity collision integrals that are calculated as described in Sec. III are shown in Fig. 10; the corresponding results that are obtained using the results [9] for H_2-H_2 are included for comparison. When the anisotropy is small, such as for H_2-H_2 interactions, both $\overline{V}(r)$ and $V_{dd'}(r)$ yield accurate values for the viscosity; note, however, that the values calculated from $V_{dd'}(r)$ provide a good approximation even for the cases with large anisotropy. Since the value of Q_n varies slowly with angular variation, this good agreement is expected from the approximation (B10) as mentioned above. In contrast, the values obtained from $\overline{V}(r)$ for large anisotropy are too large at high T.

From a consideration of the results of Appendix B and the comparisons of Fig. 10, one concludes that $V_{dd'}(r)$ provides values for $V_e(r)$ that yield transport properties for interaction of homonuclear molecules with a relatively small computational effort. Furthermore, one concludes that the additional work required to determine $\overline{V}(r)$ can be counterproductive, if one's goal is to determine transport properties.

In the remainder of this section, we investigate additional approximations that further reduce the computational effort to obtain transport data from $V_e(r)$.

TABLE III. N_2-N_2 collision integrals (Å^2).

T (K)	$\Omega_{1,1}$	$\Omega_{1,2}$	$\Omega_{1,3}$	$\Omega_{1,4}$	$\Omega_{1,5}$	$\Omega_{2,2}$	$\Omega_{2,3}$	$\Omega_{2,4}$	$\Omega_{3,3}$
100	17.95	15.30	13.67	12.62	11.89	20.71	18.42	16.75	16.60
150	15.04	13.01	11.86	11.14	10.65	17.31	15.46	14.26	14.03
200	13.66	12.01	11.11	10.55	10.16	15.54	14.07	13.16	12.87
300	12.23	11.05	10.39	9.94	9.63	13.72	12.72	12.08	11.77
400	11.45	10.47	9.94	9.60	9.33	12.78	12.02	11.58	11.15
600	10.60	9.85	9.40	9.04	8.74	11.80	11.24	10.84	10.50
800	10.07	9.39	8.87	8.65	8.42	11.25	10.70	10.43	9.98
1000	9.79	9.17	8.76	8.45	8.18	10.94	10.54	10.22	9.84
1200	9.46	8.88	8.47	8.15	7.88	10.67	10.25	9.92	9.54
1500	9.07	8.52	8.11	7.79	7.52	10.30	9.88	9.54	9.18
2000	8.60	8.05	7.65	7.34	7.08	9.82	9.40	9.08	8.71
3000	7.94	7.42	7.03	6.72	6.46	9.16	8.76	8.45	8.07
4000	7.49	6.97	6.59	6.31	6.11	8.70	8.31	8.03	7.64
6000	6.87	6.36	6.01	5.69	5.69	8.08	7.68	7.36	7.04
8000	6.43	5.90	5.63	5.54	5.32	7.58	7.34	7.28	6.69
10000	6.06	5.64	5.40	5.13	4.81	7.32	7.10	6.81	6.46

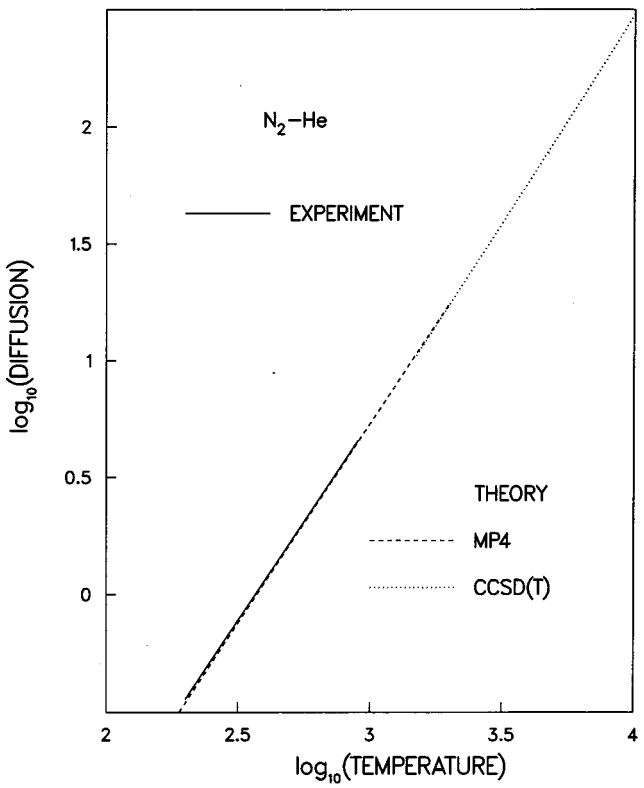

FIG. 9. The diffusion in units of cm^2/s as a function of temperature in K at a pressure of 1 atm for N_2-He interactions. The solid line represents the measured values from the correlation of Ref. [28]. The dashed and dotted lines are obtained from calculations using the potential-energy surface of Ref. [25] and $V(r,\theta_0)$ from the present calculations, respectively.

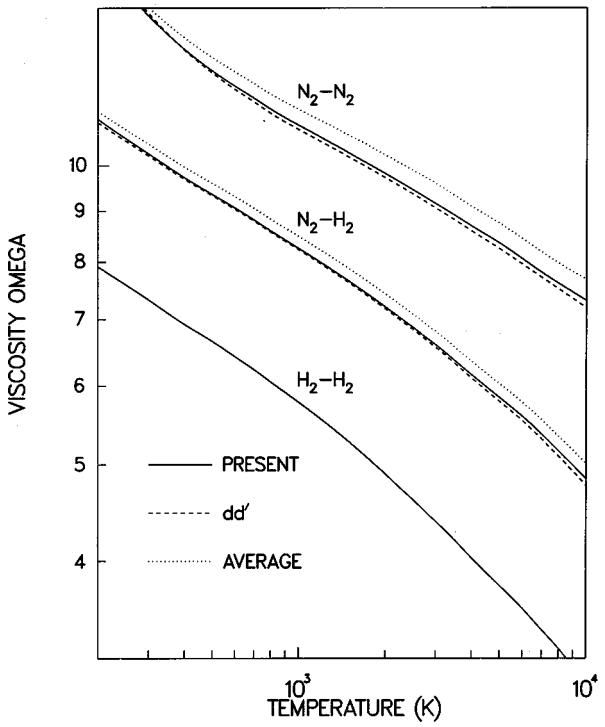

FIG. 10. The values of $\Omega_{2,2}(T)$ in units of $Å^2$ as a function of temperature in K for the collisions of H_2 and N_2. The solid lines were calculated using the sudden approximation as described in the text. The dashed and dotted curves were obtained from $V_{dd'}(r)$ and $\overline{V}(r)$, respectively; for H_2-H_2, these curves are hidden by the solid curve.

B. Universal collision integrals

Two-parameter formulations have been devised [27,28] for transport coefficients that reproduce the measured transport data; however, we have shown in Sec. II that these parameters may not be related to a physically meaningful potential-energy curve. In the following work, we examine relationships among the $V_e(r)$ calculated for various interactions and establish a theoretical formulation of the transport coefficients that is based on realistic potential energies.

A simple universal potential-energy function, such as that shown in Fig. 2 of Ref. [1], is constructed from two scaling parameters. Following correlation studies [28], we choose the Lennard-Jones parameters σ [for which $V(\sigma)=0$] and the potential well depth ϵ to scale the length and energy, respectively. The accuracy of transport properties and virial coefficients calculated from accurate *ab initio* He-He potential energies exceeds that of the best measurements [61]. We select the He-He potential function of Janzen and Aziz [62], which is based on the results of calculations [63] with symmetry-adapted perturbation theory (SAPT) and agrees well with the results of a recent supermolecule calculation [64], to represent a universal potential-energy function. The reduced potential-energy curve $V(r)/\epsilon$ for He-He is shown in Figs. 11 and 12 for large and small values of the reduced separation distance r/σ, respectively. The reduced potential energies that are based on the results of accurate *ab initio* calculations are also shown for comparison. The results for He-N_2 and N_2-N_2 are obtained from the $V_e(r)$ described above, i.e., the $V(r,\theta_0)$ of Sec. II and $V_{dd'}(r)$ from the VS method [7], respectively. The fairly good agreement of the *ab initio* and He-He results indicates that universal collision integrals derived from the He-He interaction would provide a reasonable estimate of transport properties from the two parameters σ and ϵ obtained from the potential-energy wells of $V_e(r)$.

The expansion coefficients a_n for the reduced universal collision integral $\Omega^\star$ expressed in the form

$$\ln(\Omega^\star)=\sum_{n=0} a_n[\ln(T^\star)]^n, \tag{10a}$$

where the reduced temperature is

$$T^\star=T/\epsilon, \tag{10b}$$

are calculated to second order [27] from the He-He potential-energy of Ref. [62]; the values are listed in Table IV for diffusion and viscosity. The collision integrals for a particular interaction with parameters σ and ϵ are obtained from Eq. (10) and Table IV using

$$\Omega(T)=\sigma^2\Omega^\star(T/\epsilon) \tag{11}$$

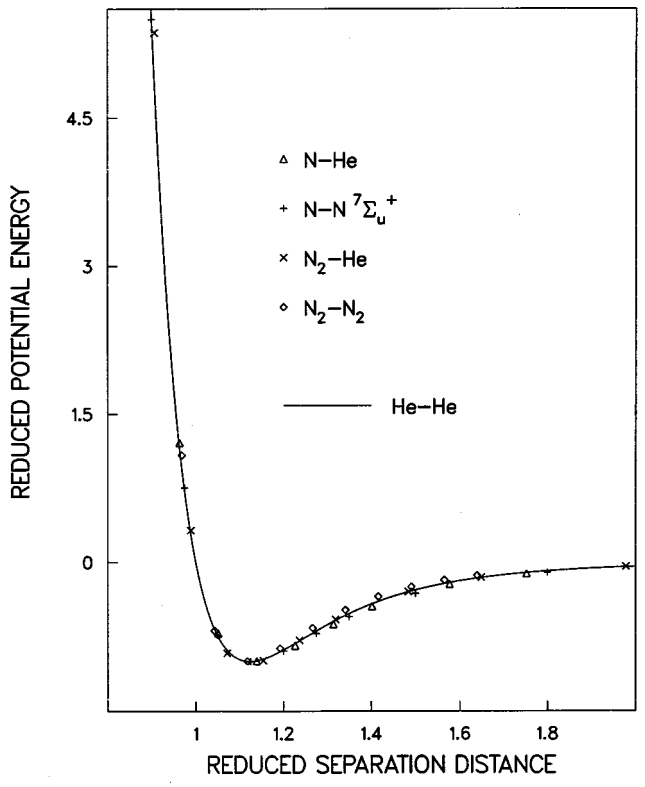

FIG. 11. Reduced potential-energy curves as a function of the reduced separation distance at large r. The solid curve is obtained from the He-He interaction energy of Ref. [62]. The data points are obtained from accurate calculations [3] of the atom-atom potential-energy and the $V_e(r)$ described in the text.

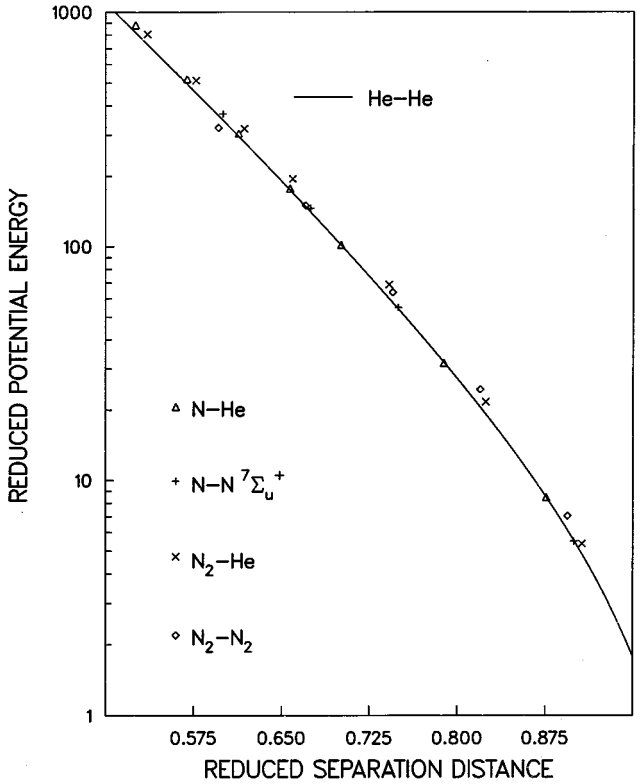

FIG. 12. Reduced potential-energy curves at small r. The solid curve and the data points are the same as those described in Fig. 11.

and are expressed in units of $Å^2$ when σ and ϵ/κ are in units of Å and K, respectively.

C. Aufbau relations

Combining relations have been devised [65–67] for the parameters of certain potential-energy functions. The combining relations [65] and measured $B(T)$ data have been applied to determine parameters [28] that reproduce the measured data for transport properties using a universal formulation. The linear behavior of $\ln V_{\mathrm{SR}}^c$ discussed in Sec. II and a consideration of the semiempirical approach of Ref. [28] leads one to construct a generalization that is based on the actual $V_e(r)$ that are determined from *ab initio* energies.

Accurate H-N potential energies that are primarily repulsive can be constructed [1], using long-range coefficients and the combining relations of Smith [66] derived for a repulsive interaction, from accurate *ab initio* H-H and N-N potential energies. In the following work, we adapt the atom-atom procedure [1] to include $V_e(r)$ for molecular interactions.

In general, we propose that the potential energy $V_e^{b\text{-}b}(r)$ for determining transport data for b-b interactions can be readily constructed (built up) using the following Aufbau procedure. First, two pairs of repulsive parameters A and ρ are determined [1] using the form (A1) from the known quantities $V^{a\text{-}a}(r)$ and $V^{b\text{-}a}(r)$, where the superscript a represents a relatively simple system such as He, and known long-range coefficients. Then, the repulsive parameters that describe $V_{\mathrm{SR}}^{b\text{-}b}(r)$ are calculated from the combining relations

$$\rho^{b\text{-}b} = 2\rho^{b\text{-}a} - \rho^{a\text{-}a} \tag{12a}$$

and

$$\rho^{b\text{-}b}\ln\left(\frac{A^{b\text{-}b}}{\rho^{b\text{-}b}}\right) = 2\rho^{b\text{-}a}\ln\left(\frac{A^{b\text{-}a}}{\rho^{b\text{-}a}}\right) - \rho^{a\text{-}a}\ln\left(\frac{A^{a\text{-}a}}{\rho^{a\text{-}a}}\right). \tag{12b}$$

Finally, $V_e^{b\text{-}b}(r)$ is obtained using Eq. (A1) to combine $V_{\mathrm{SR}}^{b\text{-}b}(r)$ and the $V_{\mathrm{DLR}}^{b\text{-}b}(r)$ that is obtained from known coefficients for the long-range forces.

The Aufbau procedure and the universal transport formulation are tested using the interaction energies described above and the N_2-N_2 long-range coefficients of Ref. [7]. In the molecule-molecule method, the system a represents H_2; the input quantities $V^{\mathrm{H_2\text{-}H_2}}(r)$ and $V^{\mathrm{N_2\text{-}H_2}}(r)$ are represented by the $V_{dd'}(r)$ obtained from the interaction energy of Ref.

TABLE IV. Coefficients a_n for universal collision integrals.

n	$\ln \Omega_{1,1}^{\star}$	$\ln \Omega_{2,2}^{\star}$
0	0.3314843	0.4376297
1	−0.5014776	−0.5310961
2	0.1443690	0.1748287
3	−0.0286224	−0.0359928
4	0.0019269	0.0025472

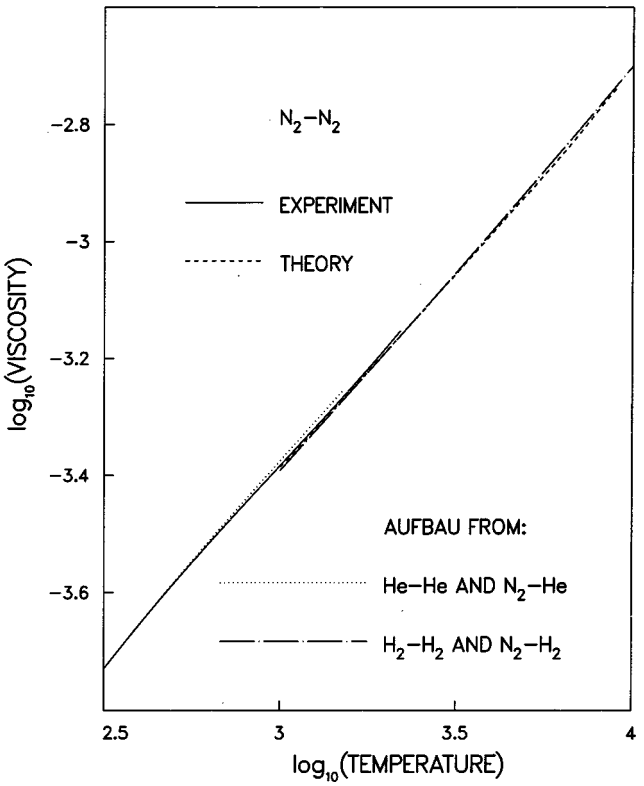

FIG. 13. The viscosity in units of gm/(cm s) as a function of temperature in K for N_2-N_2 interactions. The solid curve is obtained from measurements [59]. The dashed curve was calculated from the Ω of Table III and includes a second-order correction [27] for a pure nitrogen gas. The dash-dotted curve and the dotted curve are results of the Aufbau approximations for molecule-molecule and atom-molecule methods, respectively, that are described in the text.

[9] and the calculated results described above, respectively. The transport data are then calculated directly from the Aufbau result for $V_e^{N_2\text{-}N_2}(r)$ using the scattering methods described above. In the atom-molecule method, the system *a* represents He; the input quantities $V^{He\text{-}He}(r)$ and $V^{N_2\text{-}He}(r)$ are obtained from Ref. [62] and are represented by the results for $V(r,\theta_0)$ described above for N_2-He interactions, respectively. In this case, the two parameters σ and ϵ are determined from $V_e^{N_2\text{-}N_2}(r)$ and then used to readily calculate the N_2-N_2 transport data using the expansion for the $\Omega^\star$ of Eq. (10) and the values of a_n listed in Table IV.

In Fig. 13, the results for the viscosity that is obtained for both Aufbau methods are compared with the measured data available at low T and the results from the present calculation.

V. CONCLUSIONS

N_2-He and N_2-H_2 interaction energies are computed by *ab initio* methods in Sec. II. Our results show that the near linear behavior of $\ln V_{SR}$ obtained from the general formulation of Appendix A allows an efficient determination of the interaction energy with small computational effort when the long-range forces are known.

In Sec. III, we find that values of $B(T)$, scattering cross sections, and diffusion coefficients calculated from the interaction energies for the KKU orientations of N_2-H_2 compare well with the corresponding measured data. Collision integrals for N_2-H_2 and N_2-N_2 that allow a determination of transport properties to second order are tabulated.

In Sec. IV, we demonstrate that the interaction energies for the θ_0 and the dd' orientations are effective potential energies that yield accurate approximations to the transport properties of atom-molecule and molecule-molecule interactions, respectively. Furthermore, we present a tabulation of coefficients that readily allows the transport properties to be determined from the Lennard-Jones parameters that describe the well of these effective potential energies. Moreover, we develop an Aufbau method that allows the determination of the effective potential energies for molecular interactions from the interaction energies of simpler systems.

The identification and construction of effective potential energies presented here allows a large reduction in the computational effort required to determine transport properties. In addition, the results of the present study should provide a useful guide for the determination of the effective potential energies required for the interactions of larger molecules with more complex symmetry, where calculations by conventional methods are not feasible.

ACKNOWLEDGMENT

Support to Eugene Levin was provided by Contract No. NAS2-99092 from NASA to the Eloret Corporation.

APPENDIX A: GENERALIZED POTENTIAL-ENERGY FUNCTION

Our calculated potential energies that are primarily repulsive can be conveniently analyzed or fitted well by a functional form that has been adapted [7,8] from the result developed by Tang and Toennies [35] for an atom-atom van der Waals interaction. The modified potential-energy is expressed by the sum

$$V_{MTT}(r,\boldsymbol{\omega}) = V_{SR}(r,\boldsymbol{\omega}) + V_{DLR}(r,\boldsymbol{\omega}) \tag{A1a}$$

for each orientation specified by the angles $\boldsymbol{\omega}$. The short-range repulsive energy V_{SR} and the damped long-range attractive energy V_{DLR} have the forms

$$\ln V_{SR}(r,\boldsymbol{\omega}) = \ln[A(\boldsymbol{\omega})] - r/\rho(\boldsymbol{\omega}), \tag{A1b}$$

$$V_{DLR}(r,\boldsymbol{\omega}) = -\sum f_n[r/\rho(\boldsymbol{\omega})]\frac{C_n(\boldsymbol{\omega})}{r^n}. \tag{A1c}$$

The quantities A and ρ characterize the strength and range, respectively, of the repulsive energy. The quantities $C_n(\boldsymbol{\omega})$ are the coefficients of the long-range forces and the damping function f_n is obtained from an incomplete gamma function [68] of order $n+1$, i.e.,

$$f_n(x) = 1 - \exp(-x)\sum_{k=0}^{n}\frac{x^k}{k!}. \tag{A1d}$$

The short-range constants required for V_{MTT} can be calculated [35,67] from the parameters that locate the minimum of the potential-energy. We find, however, that an iterative procedure which does not require prior knowledge of the well parameters, but only a few values of $V(r,\boldsymbol{\omega})$, converges rapidly. An initial value $0.5a_0$ for ρ allows satisfactory convergence for all interactions that we have studied.

APPENDIX B: KOIDA-KIHARA ORIENTATIONS FOR INTERACTION OF UNLIKE MOLECULES

We consider a function $F(\theta_a,\theta_b,\phi)$ that has the same symmetry properties as the molecule formed from the interacting homonuclear diatomic molecules *a* and *b*; hence, it can be expanded in polynomials in the form

$$F(\theta_a,\theta_b,\phi)=\sum c_{L_aL_bM}d_{L_aL_bM}(\theta_a,\theta_b,\phi), \tag{B1}$$

where only zero or even values of L_a and L_b are allowed. For example, the coefficients $c_{L_aL_bM}$ are the same as those contained in Eq. (5) if F is the potential-energy. The angles θ and ϕ are defined in Sec. II and the $d_{L_aL_bM}$ are related to spherical harmonics by Eq. (6).

For terms with $L_a\neq L_b$, it is convenient to write the sum of the pairs from Eq. (B1) with the same value of M as

$$c_{L_aL_bM}d_{L_aL_bM}+c_{L_bL_aM}d_{L_bL_aM}=c^{+}_{L_aL_bM}d^{+}_{L_aL_bM}+c^{-}_{L_aL_bM}d^{-}_{L_aL_bM}, \tag{B2}$$

where we define

$$c^{\pm}_{L_aL_bM}=[c_{L_aL_bM}\pm c_{L_bL_aM}]/2, \tag{B3}$$

and noting from the relation (5) that

$$d_{L_bL_aM}(\theta_a,\theta_b,\phi)=d_{L_aL_bM}(\theta_b,\theta_a,\phi), \tag{B4}$$

we obtain

$$d^{\pm}_{L_aL_bM}(\theta_a,\theta_b,\phi)=d_{L_aL_bM}(\theta_a,\theta_b,\phi)\pm d_{L_aL_bM}(\theta_b,\theta_a,\phi). \tag{B5}$$

Hence, we have separated the expansion (B1) into pairs that are symmetric or antisymmetric with respect to interchange of the molecules *a* and *b*, e.g., from Eq. (B5) one finds

$$d^{\pm}_{L_aL_bM}(\theta_a,\theta_b,\phi)=\pm d^{\pm}_{L_aL_bM}(\theta_b,\theta_a,\phi). \tag{B6}$$

To calculate the coefficients of the expansion (B1), we define the sum and difference

$$F^{\pm}(\theta_a,\theta_b,\phi)=[F(\theta_a,\theta_b,\phi)\pm F(\theta_b,\theta_a,\phi)]/2. \tag{B7}$$

Combining Eqs. (B1), (B2), and (B7),

$$F^{\pm}(\theta_a,\theta_b,\phi)=\sum c^{\pm}_{L_aL_bM}D^{\pm}_{L_aL_bM}(\theta_a,\theta_b,\phi), \tag{B8}$$

where the terms of Eq. (B1) for $L_a=L_b$ are contained in the sum for F^{+}. Using Eqs. (B5), we can write

$$D^{\pm}_{L_aL_bM}(\theta_a,\theta_b,\phi)=\left(\frac{2-\delta_{L_aL_b}}{2}\right)d^{\pm}_{L_aL_bM}(\theta_a,\theta_b,\phi). \tag{B9}$$

The coefficients $c^{-}_{L_aL_bM}$ vanish for like molecules *a* and *b*.

The quantity c_{000} is the spherical average $\overline{F}$ and is contained in the set of coefficients c^{+}; hence, only the set of equations for F^{+} obtained from Eq. (B8) for the various orientations require a simultaneous solution to determine $\overline{F}$ for either like or unlike molecules. According to Eqs. (B8) and (B9), we can adapt the relation on p. 45 of Ref. [36] derived for the interaction of like molecules to approximate $\overline{F}$ for the interactions of unlike molecules simply by replacing $F(\theta_a,\theta_b,\phi)$ in terms for $\theta_a\neq\theta_b$ by $F^{+}(\theta_a,\theta_b,\phi)$. For an expansion in spherical harmonics with $L\leqslant 2$,

$$\overline{F}\approx F_{dd'}, \tag{B10}$$

and for $L\leqslant 4$, the result of Ref. [36] becomes

$$\overline{F}\approx\frac{4}{25}S_1+\frac{6}{25}S_2+\frac{9}{25}S_3, \tag{B11a}$$

$$S_1=\frac{1}{9}F_{zz}+\frac{2}{9}(F_{zx}+F_{xz})+\frac{2}{9}F_{xx}+\frac{1}{9}(F_{xy}+F_{yx}), \tag{B11b}$$

$$S_2=\frac{1}{3}(F_{zd}+F_{dz})+\frac{2}{3}(F_{xd}+F_{dx}), \tag{B11c}$$

$$S_3=\frac{1}{4}F_{dd}+\frac{1}{2}F_{dd'}+\frac{1}{4}F_{dd''}. \tag{B11d}$$

One can show that small [69] contributions from the terms for d_{222} and d_{444} have been neglected on the right-hand-side of relations (B10) and (B11a), respectively.

Furthermore, the selection [36] of orientations to approximate $\overline{F}$ is based on the symmetry properties of F; thus, it follows that Eqs. (B11) should yield accuracy of $\overline{F}$ for unlike molecules that is comparable to that obtained for like molecules.

According to Eqs. (B7)–(B9), the potential-energy surface can be expressed

$$V(r,\theta_a,\theta_b,\phi)=\sum [v^{+}_{L_aL_bM}(r)D^{+}_{L_aL_bM}(\theta_a,\theta_b,\phi)+v^{-}_{L_aL_bM}(r)d^{-}_{L_aL_bM}(\theta_a,\theta_b,\phi)], \tag{B12}$$

where $v^{\pm}(r)$ specifies the variation with separation distance. For like molecules, the c^{-} vanish, as mentioned above, and the expansion (B12) reduces to the result applied in Ref. [7]. Lastly, we point out that the determination of the coefficients from the values for V for selected orientations then reduces to solving the two sets of simultaneous equations obtained for each symmetry, e.g., Eqs. (B8) can be applied to obtain one set of equations for the v^{+} and another for the v^{-}.

APPENDIX C: SCATTERING FOR LARGE l

The small-angle sudden scattering cross sections for the $V(r,\boldsymbol{\omega})$ of Sec. II with small values of γ are compared below with the corresponding results obtained from $\overline{V}(r)$ using approximations developed for scattering in a central-field potential.

For large values of l such that V/E is small compared to 1 over the range of integration, the series expansion of Smith *et al.* [70] provides a useful approximation to evaluate the scattering produced by long-range forces. From their results, the JWKB phase shift can be expressed in the form [71]

$$\eta=\frac{k}{2}\int_{b^2}^{\infty}F(z)(z-b^2)^{1/2}dz, \tag{C1}$$

where

$$F(z)=\sum_{n=0}^{\infty}\frac{1}{\Gamma(n+2)}\frac{d^{n+1}}{dz^{n+1}}\left[z^n\left(\frac{V(z^{1/2})}{E}\right)^{n+1}\right] \tag{C2}$$

and the impact parameter b satisfies the semiclassical relation

$$b=(l+1/2)/k. \tag{C3}$$

When the potential falls off as an inverse power of r for large r, i.e.,

$$V(r,\boldsymbol{\omega})\rightarrow C_{\nu}(\boldsymbol{\omega})/r^{\nu}, \tag{C4}$$

the integration of Eq. (C2) can be carried out analytically and the phase shift becomes

$$\eta=\frac{l}{k}\sum_{n=0}^{\infty}\frac{\Gamma\left(\frac{n+2}{2}\nu-\frac{1}{2}\right)\Gamma\left(\frac{1}{2}\right)}{\Gamma(n+2)\Gamma\left(\frac{n+1}{2}\nu-n\right)}\left[-\frac{C_{\nu}}{E}\left(\frac{k}{l}\right)\right]^{n+1}. \tag{C5}$$

This series converges absolutely when

$$\frac{(\nu/2)^{\nu/2}}{(\nu/2-1)^{\nu/2}}\left(\frac{k}{l}\right)^{\nu}\frac{|C_{\nu}|}{E}<1. \tag{C6}$$

For small scattering angles θ, the scattering amplitude can be approximated by a power series in θ^2. Taking the first term of Eq. (C5), the scattering amplitude can be integrated analytically [72] to obtain

$$f(E,\theta,\boldsymbol{\omega})=-\frac{\pi}{2(\nu-1)k}\sum_{n=0}\frac{(-1)^n}{[\Gamma(n+1)]^2}\frac{(G_{\nu})^{2[(n+1)/(\nu-1)]}}{\Gamma\left(2\frac{n+1}{\nu-1}+1\right)}\times H_{n\nu}\left(\frac{\theta}{2}\right)^{2n}, \tag{C7}$$

where

$$G_{\nu}(E,\boldsymbol{\omega})=\frac{\Gamma(1/2)\Gamma\left(\frac{\nu-1}{2}\right)}{2\Gamma(\nu/2)}\frac{|C_{\nu}(\boldsymbol{\omega})|}{E}k^{\nu}, \tag{C8}$$

$$H_{n\nu}(\boldsymbol{\omega})=\frac{C_{\nu}(\boldsymbol{\omega})/|C_{\nu}(\boldsymbol{\omega})|}{\cos\left(\frac{n+1}{\nu-1}\pi\right)}-\frac{i}{\sin\left(\frac{n+1}{\nu-1}\pi\right)}. \tag{C9}$$

The index n is restricted to positive integers less than $(\nu-3)/2$ and $\nu-2$ in the real and imaginary parts, respectively, of Eq. (C7).

For larger values of θ, we consider the results from the semiclassical analysis of Ford and Wheeler [73]. The nth partial scattering amplitude is

$$f_n(E,\theta,\boldsymbol{\omega})=\sigma_n^{1/2}\exp(i\beta_n), \tag{C10}$$

where partial cross sections σ_n and the phases β_n are determined from the nth point of the stationary phase of the scattering amplitude (where the sum is replaced by an integral). The analog to the classical scattering cross section is

$$\sigma=\frac{1}{2k\sin\theta}\frac{l+1/2}{|\eta''|}, \tag{C11a}$$

$$\beta=2\eta-2(l+1/2)\eta'+(|\eta''|/\eta\pm1)\pi/4+(1\pm1)\pi/2-m\pi, \tag{C11b}$$

where the stationary phase value l_n is obtained from

$$2\eta'+2m\pi\pm\theta=0, \tag{C12}$$

and m is an integer. The primes indicate derivatives with respect to l, and m is zero or a positive/negative integer.

The cross section for the orientation specified by $\boldsymbol{\omega}$ is obtained from

$$\sigma(E,\theta,\boldsymbol{\omega})=|f(E,\theta,\boldsymbol{\omega})|^2. \tag{C13}$$

The value of the observed cross section of $\overline{\sigma}(E,\theta)$ is obtained by the appropriate integral [53] of $\sigma(E,\theta,\boldsymbol{\omega})$ over all orientations $\boldsymbol{\omega}$.

We next consider applications to molecular collisions such as the N_2-H_2 scattering described in Sec. II. For suffi-

ciently large E, the contribution to $f(E,\theta,\boldsymbol{\omega})$ from the r^{-5} potential-energy terms is not appreciable, i.e., the η for the large l, where the quadrupole-quadrupole force provides the dominant interaction, are too small. The largest contribution to η at smaller l comes from the dispersion forces in the region of r near the value of b obtained from Eq. (C3). The values of γ that describe the anisotropy of the dispersion coefficients for N_2-H_2 interactions in Eq. (7) are found to be small. Hence, the scattering amplitude of Eq. (C7) can be expanded in powers of γ; one can note from Eqs. (C7) and (C13) that the contribution from the first-order terms of the expansion to $\bar{\sigma}$ vanishes due to the orthogonality of the associated Legendre functions. Hence, a first-order approximation to $\bar{\sigma}$ depends only on the C^{ν}_{000}, which (as pointed out in Sec. II) are also the dispersion coefficients for $\bar{V}$. A similar conclusion can be obtained by expanding the ratio $(l+1/2)/|\eta''|$ of Eq. (C11) in γ and combining the result to obtain $\bar{\sigma}$ in a similar manner. Hence, one concludes that the cross section obtained using the sudden approximations is nearly the same as that obtained from $\bar{V}(r)$ at small θ, if the values of γ are small.

[1] J.R. Stallcop, C.W. Bauschlicher, H. Partridge, S.R. Langhoff, and E. Levin, J. Chem. Phys. **97**, 5578 (1992).
[2] E. Levin, H. Partridge, and J.R. Stallcop, J. Thermophys. Heat Transfer **4**, 469 (1990).
[3] J. R. Stallcop, H. Partridge, A. Pradhan, and E. Levin, J. Thermophys. Heat Transfer (to be published).
[4] H. Partridge, C.W. Bauschlicher, J.R. Stallcop, and E. Levin, J. Chem. Phys. **99**, 5951 (1993).
[5] S.P. Walch, J. Chem. Phys. **93**, 2384 (1990).
[6] J.R. Stallcop, H. Partridge, S.P. Walch, and E. Levin, J. Chem. Phys. **97**, 3431 (1992).
[7] J.R. Stallcop and H. Partridge, Chem. Phys. Lett. **281**, 212 (1997).
[8] J.R. Stallcop, H. Partridge, and E. Levin, Chem. Phys. Lett. **254**, 25 (1996).
[9] J.R. Stallcop, E. Levin, and H. Partridge, J. Thermophys. Heat Transfer **12**, 514 (1998).
[10] J. R. Stallcop, H. Partridge, and E. Levin (unpublished).
[11] *Computational Modeling in Semiconductor Processing*, edited by M. Meyyapan, (Artech House, Boston, 1995).
[12] J.R. Stallcop, H. Partridge, and E. Levin, Phys. Rev. A **53**, 766 (1996).
[13] R.J. Bartlett, Annu. Rev. Phys. Chem. **32**, 359 (1981).
[14] K. Raghavachari, G.W. Trucks, J.A. Pople, and M. Head-Gordon, Chem. Phys. Lett. **157**, 479 (1989).
[15] T.H. Dunning, J. Chem. Phys. **90**, 1007 (1989).
[16] R.A. Kendall, T.H. Dunning, and R.J. Harrison, J. Chem. Phys. **96**, 6796 (1992).
[17] D.E. Woon, K.A. Peterson, and T.H. Dunning, J. Chem. Phys. **98**, 1358 (1993).
[18] T. Vladimiroff, J. Phys. Chem. **77**, 1983 (1973).
[19] P.G. Burton, N.R. Carlson, and E.A. Magnusson, Mol. Phys. **32**, 1687 (1976).
[20] J.S. Wright and V.J. Barclay, J. Chem. Phys. **86**, 3054 (1987).
[21] C.W. Bauschlicher and H. Partridge, J. Chem. Phys. **109**, 4707 (1998).
[22] F-M. Tao and Y-K. Pan, J. Chem. Phys. **97**, 4989 (1992).
[23] H. Partridge and C.W. Bauschlicher, Mol. Phys. **96**, 705 (1999).
[24] S.F. Boys and F. Bernardi, Mol. Phys. **19**, 533 (1970).
[25] C-H. Hu and A.J. Thakkar, J. Chem. Phys. **104**, 2541 (1996).
[26] J. Kestin, S.T. Ro, and W.A. Wakeham, J. Chem. Phys. **56**, 4036 (1972).
[27] G. C. Maitland, M. Rigby, E. B. Smith, and W. A. Wakeham, *Intermolecular Forces. Their Origin and Determination* (Oxford University Press, Oxford, 1981).
[28] J. Bzowski, J. Kestin, E.A. Mason, and F.J. Uribe, J. Phys. Chem. Ref. Data **19**, 1179 (1990).
[29] W.J. Meath and A. Kumar, Int. J. Quantum Chem., Symp. **24**, 501 (1990).
[30] H. Hettema, P.E.S. Wormer, and A.J. Thakkar, Mol. Phys. **80**, 533 (1993).
[31] D.M. Bishop and J. Pipin, Int. J. Quantum Chem. **45**, 349 (1993).
[32] C. Graham, D.A. Imrie, and R.E. Raab, Mol. Phys. **93**, 49 (1998).
[33] J.M.M. Roco, A. Calvo Hernández, S. Velasco, and A. Medina, J. Chem. Phys. **110**, 5218 (1999).
[34] K.T. Tang, J.P. Toennies, and C.L. Yiu, Phys. Rev. Lett. **74**, 1546 (1995).
[35] K.T. Tang and J.P. Toennies, J. Chem. Phys. **80**, 3726 (1984).
[36] A. Koida and T. Kihara, Chem. Phys. **5**, 34 (1974).
[37] J.R. Stallcop, H. Partridge, and E. Levin, Phys. Rev. A **53**, 766 (1996).
[38] J. O. Hirschfelder, J. F. Curtiss, and R. B. Bird, *Molecular Theory of Gases and Liquids* (Wiley-Interscience, New York, 1964).
[39] J.D. Poll and L. Wolniewicz, J. Chem. Phys. **68**, 3053 (1978).
[40] G. Karl, J.D. Poll, and L. Wolniewicz, Can. J. Phys. **53**, 1781 (1975).
[41] F. Visser, P.E.S. Wormer, and P. Stam, J. Chem. Phys. **79**, 4973 (1983).
[42] W. Rijks and P.E.S. Wormer, J. Chem. Phys. **88**, 5704 (1988).
[43] H. Partridge (unpublished).
[44] S.J. Cubley and E.A. Mason, Phys. Fluids **18**, 1109 (1975).
[45] R.E. Miller, P. Vohralik, and R.O. Watts, J. Chem. Phys. **85**, 3891 (1986).
[46] P.J. Hay, R.T. Pack, and R.L. Martin, J. Chem. Phys. **81**, 1360 (1984).
[47] R.T. Pack, J. Chem. Phys. **78**, 7217 (1978).
[48] J. Reuss and J.J.M. Beenakker, Physica (Amsterdam) **22**, 869 (1956).
[49] M.G. Ostronov, P.E. Bol'shakov, L.L. Gel'perin, and A.A. Orlova, Russ. J. Phys. Chem. **41**, 1171 (1967).
[50] P. Zandbergen and J.J.M. Beenakker, Physica (Amsterdam) **33**, 343 (1967).
[51] J. Brewer and G.W. Vaughn, J. Chem. Phys. **50**, 2960 (1969).

[52] W. Dilling and J. Schaefer, Z. Phys. D: At., Mol. Clusters **13**, 207 (1989).
[53] G.A. Parker and R.T. Pack, J. Chem. Phys. **68**, 1585 (1978).
[54] E. Levin, D.W. Schwenke, J.R. Stallcop, and H. Partridge, Chem. Phys. Lett. **227**, 669 (1994).
[55] J.R. Stallcop, H. Partridge, and E. Levin, J. Chem. Phys. **95**, 6429 (1991).
[56] C.V. Broughton, R.E. Miller, P.F. Vohralik, and R.O. Watts, Mol. Phys. **58**, 827 (1986).
[57] H.F. Vugts, A.J.H. Boerboom, and J. Los, Physica (Amsterdam) **50**, 593 (1970).
[58] A. Boushehri, J. Bzowski, J. Kestin, and E.A. Mason, J. Phys. Chem. Ref. Data **16**, 445 (1987).
[59] E. Vogel, T. Strehlow, J. Millat, and W.A. Wakeham, Z. Phys. Chem. (Leipzig) **270**, 1145 (1989).
[60] T.R. Marrero and E.A. Mason, J. Phys. Chem. Ref. Data **1**, 3 (1972).
[61] R.A. Aziz, A.R. Janzen, and M.R. Moldover, Phys. Rev. Lett. **74**, 1586 (1995).
[62] A.R. Janzen and R.A. Aziz, J. Chem. Phys. **107**, 914 (1997).
[63] T. Korona, H.L. Williams, R. Bukowski, R. Jeziorski, and K. Szalewicz, J. Chem. Phys. **106**, 5109 (1997).
[64] T. van Mourik and T.H. Dunning, J. Chem. Phys. **111**, 9248 (1999).
[65] J. Bzowski, E.A. Mason, and J. Kestin, Int. J. Thermophys. **9**, 131 (1988).
[66] F.T. Smith, Phys. Rev. A **5**, 1708 (1972).
[67] K.T. Tang and J.P. Toennies, Z. Phys. D: At., Mol. Clusters **1**, 91 (1986).
[68] A. Erdélyi, W. Magnus, F. Oberhettinger, and F. G. Tricomi, *Higher Transcendental Functions* (McGraw Hill, New York, 1953), Vol. II, Chap. 9.
[69] J. Schaefer and W.E. Köler, Z. Phys. D: At., Mol. Clusters **13**, 217 (1989).
[70] F.T. Smith, R.P. Marchi, and K.G. Dedrick, Phys. Rev. **150**, 79 (1966).
[71] J. R. Stallcop, NASA SP-3052, Scientific and Technical Information Division, 1969.
[72] E.A. Mason, J.T. Vanderslice, and C.J.G. Raw, J. Chem. Phys. **40**, 2153 (1964).
[73] K.W. Ford and J.A. Wheeler, Appl. Phys. **7**, 259 (1957).